Published in final edited form as:
Structure. 2012 April 4; 20(4): 729–741. doi:10.1016/j.str.2012.02.021.

An Asymmetry-to-Symmetry Switch in Signal Transmission by the Histidine Kinase Receptor for TMAO

Jason O. Moore[1] and **Wayne A. Hendrickson**[1,2,3,*]

[1]Department of Biochemistry and Molecular Biophysics, Columbia University, New York, NY 10032 USA

[2]Department of Physiology and Cellular Biophysics, Columbia University, New York, NY 10032 USA

[3]Howard Hughes Medical Institute, Columbia University, New York, NY 10032 USA

Summary

The osmoregulator trimethylamine-N-oxide (TMAO), commonplace in aquatic organisms, is used as the terminal electron acceptor for respiration in many bacterial species. The TMAO reductase (Tor) pathway for respiratory catalysis is controlled by a receptor system that comprises the TMAO-binding protein TorT, the sensor histidine kinase TorS and the response regulator TorR. Here we study the TorS/TorT sensor system to gain mechanistic insight into signaling by histidine kinase receptors. We determined crystal structures for complexes of TorS sensor domains with apo TorT and with TorT(TMAO); we characterized TorS sensor associations with TorT in solution; we analyzed the thermodynamics of TMAO binding to TorT-TorS complexes; and we analyzed in vivo responses to TMAO through the TorT/TorS/TorR system to test structure-inspired hypotheses. TorS-TorT(apo) is an asymmetric 2:2 complex that binds TMAO with negative cooperativity to form a symmetric active kinase.

INTRODUCTION

Trimethylamine-N-oxide (TMAO) is present at high concentrations in many aquatic organisms and in renal glands where it is used as an osmoregulator and counterbalance to the denaturing effects of urea (Barrett and Kwan, 1985). Many species of aquatic bacteria use TMAO as a terminal electron receptor in anaerobic respiration or during exponential growth under aerobic conditions (Ansaldi et al., 2007). The TMAO reductase (Tor) pathway for TMAO-based respiration has two parts: a regulatory two-component pathway and a catalytic respiration pathway.

*Correspondence: wayne@convex.hhmi.columbia.edu.

SUPPLEMENTAL DATA

Supplemental Data include Extended Experimental Procedures, five figures, and three tables, and can be found with this article online at xxx.

ACCESSION NUMBERS

Atomic coordinates and structure factors have been deposited in the Protein Data Bank (http://www/rcsb/pdb) with accession codes 3O1H, 3O1I and 3O1J as identified in Table 1.

Two-component systems, which prevail for signaling in prokaryotes and many other protists, characteristically comprise a sensor histidine kinase and its cognate response regulator. The Tor pathway also has a third component: the periplasmic binding protein TorT where TMAO actually binds (Baraquet et al., 2006). TorT associates as a co-receptor with the histidine kinase receptor TorS to form the sensor complex. TMAO-stimulated TorS phosphorylates the response regulator TorR (Simon et al., 1994); and phosphorylated TorR activates transcription from the *torCAD* operon (Simon et al., 1995). The *torCAD* operon encodes the c-type cytochrome TorC (Gon et al., 2001), the TMAO-terminal reductase TorA (Méjean et al., 1994) and TorD, a TorA-specific chaperone (Ilbert et al., 2004).

TorS has all elements that typify histidine kinase receptors. Its extracellular sensor domain (Cheung and Hendrickson, 2010) is positioned between two N-terminal transmembrane helices, and its cytoplasmic portion includes the canonical core (Marina et al., 2005; Stewart, 2010) of a helical dimerization domain, a phosphor-accepting histidine residue, and the signature catalytic kinase domain (Wolanin et al., 2002). These essential cytoplasmic domains are sandwiched between the commonplace HAMP domain (Hulko et al., 2006) and a phospho-relay pair (Jourlin et al., 1997). Histidine phosphorylation ensues when TorS is stimulated by TMAO; then, following a phophotransfer cascade, aspartyl-phosphorylated TorR dimerizes to generate an active transcription factor (Gao and Stock, 2009). Unstimulated TorS functions as a phosphatase (Ansaldi et al., 2001), reversing the phospho-relay pathway, as in other histidine kinase receptors that have both kinase and phosphatase activities (Igo et al., 1989). Indeed, in some, ligand binding stimulates phosphatase action to reverse constitutive phosphorylation in the apo state (Freeman and Bassler, 1999). The mechanism by which sensory input is transmitted across the membrane to produce one or the other response has been unclear.

We previously described crystal structures of the TorS sensor ($TorS_S$) domains from *Escherichia coli* and *Vibrio parahaemolyticus* (Moore and Hendrickson, 2009). The TorS sensors are novel α-helical proteins, but their membrane-proximal helical-bundles are topologically the same as the nitrate sensor NarX (Cheung and Hendrickson, 2009) and the chemotaxis aspartate receptor Tar (Yeh et al., 1996). Here we present crystal structures of the TorT-$TorS_S$ complex from *V. parahaemolyticus* ($vpTorS_S$ and vpTorT), both in the unliganded apo state and in complexes with TMAO and with isopropanol, an adventitious TMAO mimic. All three complexes are 2:2 heterotetramers. We also analyze the thermodynamics of oligomerization by analytical ultracentrifugation and of TMAO binding by isothermal titration calorimetry. We discovered that TorT-$TorS_S$ is asymmetric in the apo state, that it binds TMAO in two steps with a novel mechanism of negative cooperativity, and that the fully ligated complex is symmetric. This is the first histidine kinase sensor for which both the apo and ligand-bound dimeric states are characterized. Using an *in vivo* assay system that we devised for the Tor pathway of *E. coli*, we tested structure-inspired hypotheses of ligand binding and signal transmission. Based on our observations, we propose a mechanism in which an asymmetry-to-symmetry switch is responsible for signal transduction across the membrane to control kinase vs. phophatase activity in the TorS/TorR two component system.

RESULTS

Production of TorT-TorS Sensor Domain Complexes

To study the interactions among TMAO, TorT and TorS, we produced the periplasmic binding protein TorT from *V. parahaemalyticus* (vpTorT) and formed its complex with the sensor domain from the cognate histidine kinase receptor, $vpTorS_S$. We found that full-length vpTorT would bind to $vpTorS_S$, but that C-terminally truncated versions would not. Based on native gel electrophoresis and size exclusion chromatography, the complex

appeared to be a 2:2 heterotetramer, and this stoichiometry was confirmed by analytical ultracentrifugation. We initially sought to produce crystals in the apo state, without TMAO, but isopropanol from the crystallization medium was found to occupy the ligand binding site of TorT when the structure was solved. This hypothesis of adventitious binding was proved by forming and solving the structure of the authentic complex with TMAO itself. Finally, using alternative conditions devoid of isopropanol, we obtained the structure of the true apo state of the TorT-TorS$_S$ complex.

Crystallographic Analyses of the TorT-TorS$_S$ Complexes

Using multiwavelength anomalous diffraction (MAD) at the Se K-edge, we first determined the structure of selenomethionyl vpTorS$_S$ in complex with vpTorT without TMAO (Table S1). The asymmetric unit comprises one 2:2 heterotetrameric complex, which is very nearly two-fold symmetric. Each protomer is fully ordered apart from a few terminal residues and four residues in each TorT (Table 1). Unexpected electron density was found in the ostensible ligand-binding clefts of both TorT, which we identified as isopropanol based on composition of the crystallization buffer and chemical similarity to TMAO. The structure was refined against native data at 2.95 Å resolution to residuals R / R$_{free}$ of 22.6% / 24.9% (Table 1).

The vpTorS$_S$-vpTorT structure in complex with TMAO was solved by molecular replacement based on the isopropanol-bound structure. Here the asymmetric unit consists of one TorS$_S$ protomer, which we call TorS^T, and one TorT protomer, TorT^T. A crystallographic two-fold axis generates a heterotetramer that is virtually identical to the isopropanol-bound structure and its ordering is also very similar; notably, TorT^T residues 172-175 are disordered. Electron density in the ligand binding cleft of TorT^T was fitted by TMAO (Fig. S1), and the structure was refined at 3.1 Å resolution to R / R$_{free}$ = 21.8% / 25.2% (Table S1, Table 1).

The structure of the vpTorS$_S$-vpTorT complex in the apo state was solved by molecular replacement, again using the isopropanol-bound structure in the search. Two TorS$_S$ protomers, called TorS' and TorS'', and two TorT protomers, called TorT' and TorT'', constitute the asymmetric unit. The molecular architecture of this heterotetramer is like that of the ligand-bound structures, but here there is a pronounced asymmetry. In particular, TorT'' is fully ordered throughout whereas TorT' has a disordered loop as in the other structures. Apo-state TorT-TorS$_S$ was refined at 2.8 Å resolution to R / R$_{free}$ of 24.8% / 29.1% (Table S1, Table 1).

Overall Structure of the Heterotetrameric Complexes

All three TorT-TorS$_S$ complexes are similar in overall structure, typified by the identically symmetric complex with TMAO (Fig. 1). The topology of TorS$_S$ protomers in these complexes is as previously described for TorS$_S$ alone (Moore and Hendrickson, 2009), comprising a left-handed four-helix bundle inserted through helical extensions into a membrane proximal, right-handed four-helix bundle; however, the inter-bundle dispositions of vpTorS$_S$ protomers in the heterotetramers are straightened significantly (11.4-13.9°) from that in isolated vpTorS $_S$ (Fig. S2). The TorS$_S$ protomers interact with one another across the entire length of the molecular diad axis, burying a total of ~2300Å^2 for the TMAO complex (Fig. 1A). The TorT protomers make no contact with one another, but each TorT protomer interacts with both TorS$_S$ protomers in the heterotetramer. The two TorT protomers are on opposite sides, and each buries a total of ~1600Å^2 into its TorT^T:(TorS$^{T'}$-TorS$^{T''}$) interface in the TMAO complex (Fig. 1B). TorS interactions with TorT are exclusively via the distal four-helix bundles and an inter-subunit four-helix bundle tower domain (Fig. 1A).

$TorS_S$ has four distinct regions as seen in heterotetramers (Fig. 1C). Besides the proximal and distal four-helix bundles described for the monomeric crystal structures of $TorS_S$ alone, there is an inter-bundle coupler and a tower bundle. The inter-bundle coupler connects the proximal and distal bundles through helices α3 and α6. This is the only region where no contact is made between the two $TorS_S$ protomers. The α3-α4 helical-hairpin tips associate across the molecular diad axis to form a four-helix tower bundle that extends beyond the distal bundles.

Structure of Periplamic Binding Protein TorT

TorT is a periplasmic binding protein (PBP) belonging to a unique family closest in sequence to ribose binding protein (RBP) (Baraquet et al., 2006). Not surprisingly, its structure is similar to that of other PBPs (Quiocho and Ledvina, 1996) and especially so to RBP (Bjorkman and Mowbray, 1998). TorT comprises two α/β domains (Fig. 2A), each organized with similar topology (Fig. 2B). Following convention, the domains are designated N-terminal (NTD) and C-terminal domain (CTD), although the polypeptide courses back and forth through three loops (βE-α4, βJ-α10 and βK-βL) that form a hinge. The interface between the two domains forms a binding pocket. Unique to TorT, a 26-residue C-terminal extension (CTE) is added to the Type I PBP template of RBP (Fig. 2C). Apart from short helix α10, this tail has an extended conformation that, in the complexes, makes contacts with both TorT domains and also with TorS. The CTE is required for TorT binding to $TorS_S$ (Fig. S3).

The individual domains of TorT are structurally similar to the corresponding domains of *E. coli* RBP (ecRBP), but their relative dispositions and movements in response to ligand binding differ greatly. A domain-by-domain superposition of $TorT^T$ with ecRBP (PDB id: 2DRI) has 215 out of 301 (71%) of the Cα positions contiguously within 3Å of one another for a root-mean-squared deviation (RMSD) of 1.35Å. The corresponding structure-based sequence alignment shows 19.6% identity between vpTorT and ecRBP (Fig. 2C). The binding of ribose to ecRBP results in a 61° clamshell-like closure about an in ter-domain hinge onto its interfacial binding pocket (Bjorkman and Mowbray, 1998). By contrast, TorT is little changed between its apo and ligated states. The two apo domains (TorT' and TorT") have hinge angles within ± 3° from that of $TorT^T$ and all are ~15° more open than the ribose-bound s tate of RBP. Thus, the effect of ligand binding in the TorT/TorS system is much more subtle than in RBP.

The interfaces of apoTorT', apoTorT" and TorT(TMAO) with their respective TorS partners are all similar. In each complex, the CTD of TorT interacts with the distal and tower bundles of both $TorS_S$ protomers, the NTD contacts the distal bundle of only one $TorS_S$ protomer, and the CTE interacts with distal and tower bundles but only of that same $TorS_S$ protomer. Eight of the 26 CTE residues interact with TorS, notably via α10-tower contacts. TorT-TorS interactions are consistent with the essentiality of CTE for TorT-TorS binding (Fig. S3) and with resistance to proteolysis conferred by TorT binding to TorS (Baraquet et al., 2006). Other structures of PBPs with their respective partners include LuxP bound to LuxQ (Neiditch et al., 2005; Neiditch et al., 2006), ModA to $ModB_2C_2A$ (Hollenstein et al., 2007), BtuF to $BtuC_2D_2$ (Hvorup et al., 2007) and MBP to $MalFGK_2$ (Oldham et al., 2007). In each of these, the ligand binding cavity of the PBP faces its partner, whereas the binding cavity in TorT is parallel to the TorS-TorS dimer axis.

The TMAO Binding Site in TorT

TMAO binds at the interface between the NTD and CTD domains of TorT, as for ligands of other periplasmic binding proteins. This binding pocket, which is also preserved in the apo-state TorT' and TorT" subunits (Figs. 3A,B), involves two distinct sets of interactions

between TorT and TMAO (Fig. 3C). One is a hydrophilic surface from the NTD domain where functional groups from Trp45 and Tyr71 and an Asp42-coordinated water molecule all hydrogen bond to the oxygen atom of TMAO. The other is an aromatic cage formed around the quaternary amine of TMAO. This interaction is mediated by the aromatic groups of Tyr44, Trp140 and Tyr252, the latter two being from CTD. These six residues are all absolutely conserved in TorT proteins.

Another feature of the binding pocket is a flexible seven-residue loop that connects strand βF to helix α5. The loop is defined by a GPXXXGG motif where the glycines and proline are absolutely conserved in all TorT homologs. The βF-α5 loop lacks density in every protomer of TorT except for TorT", where this otherwise flexible loop is uniquely ordered (Fig. 3B).

To further analyze the binding of TMAO to TorT, we generated a β-galactosidase reporter system for TorS/TorT function in *E. coli*. A strain was created with the endogenous *torT-torS* deleted, and corresponding activities were recovered with a plasmid containing the *torT-torS* operon. This plasmid also contained a *LacZ* gene positioned so that its transcription would be regulated by the *torCAD* promoter. We made conservative mutations in the six residues that interact directly with TMAO, and found TMAO-induced activity reduced to background for all but one (Fig. 3D). It is unclear why the W59F mutation in ecTorT has no effect since Trp45 directly coordinates TMAO in vpTorT. Because of the extreme sensitivity at other sites, we further evaluated the binding pocket environment. All residues whose side chains are contacted by the hydrophilic atoms in these six residues, as well as the six themselves, are identical among all 20 known TorT proteins. Relative dispositions are essentially fixed in all states. Thus, a finely coordinated ligand-binding site appears to be vital for activity.

We also made several mutations in the GPXXXGG segment (βF-α5 loop), mainly intending to make the loop either more rigid or more flexible. All of the mutations resulted in a reduced response to TMAO, with some having a more dramatic effect than others (Fig. 3E). Gly169 has a glycine-only conformation, and its mutation eliminated the response. Mutations in either C-terminal glycine residue greatly reduced activity. Other mutations expected to increase flexibility gave reduced responses at lower concentrations of TMAO but were at or above wild type levels in higher TMAO concentrations (≥ 10 mM). We suggest a gating function for βF-α5.

Conformational Transition between Asymmetric Apo and Symmetric TMAO-bound States

The TorT-TorS$_S$ complexes with either the adventitious isopropanol or with TMAO are virtually identical. Even though the isopropanol complex has a full heterotetramer in the asymmetric unit, its two protomeric TorT-TorS$_S$ 'dimers' are related by a nearly perfect diad-axis of symmetry (rotation $\chi = 179.6°$ and screw translation $t_\chi = 0.09$Å) and an RMSD of 0.55Å between corresponding Cα positions. Moreover, the entire isopropanol complex can be superimposed onto the exactly symmetric TMAO-bound complex with a Cα RMSD of 0.55Å. Thus, here we compare only the TMAO complex with the apo-state complex, which is asymmetric ($\chi = 176.6°$, $t_\chi = 0.19$Å, Cα RMSD = 1.68 Å) and considerably different from the TMAO complex (Cα RMSD = 1.27Å overall). The transition between the apo and TMAO-bound states maintains almost all contacts between TorT and TorS subunits. One exception is contacts between residues Glu257 and Asp258 from the α5-α6 loops of TorS' and TorS^T with Arg325 of TorT' and TorT^T, which are missing where this TorS" loop is flipped away from TorT". Our mutational analysis indicates some functional sensitivity at this contact (Table S2A). Generally, structural differences are defined by a series of relative displacements between the several individual rigid domains. These displacements are small enough that they do not disrupt specific inter-residue contacts.

Asymmetry in the apo-state complex is especially noticeable in the TorT subunits, where differences are discretely localized to the inter-domain hinge angles. Structures are very similar for TorT' and TorT'' within both NTD and CTD (Cα RMSD = 0.44Å each), but the relative disposition is more open in TorT'' than in TorT'. After superposition of the two NTDs, an opening rotation of 5.0° is required to superimpose the CTD of TorT' onto that of TorT''. Relative to $TorT^T$, TorT' is 2.3° more closed and TorT'' is 2.6° more open (Figs. 4A,B), again with little variation within domains. The axes of rotation for these transformations are similar to that relating the apo and ribose-bound states of ecRBP; however, RBP is much more open (+61°) without than with its ligand (Bjorkman and Mowbray, 1998).

The disposition of TorT protomers in the TorT-$TorS_S$ complex compounds the apo-state asymmetry (Tables S3A,B). The α3-α4 tower bundle in the apo state has nearly perfect diad symmetry (χ = 179.8°, t_χ = 0.04Å), but its associated TorT molecules are asymmetric and more divergent for NTDs (χ = 174.6°, t_χ = -0.56Å), which do not contact the tower domain, than for CTDs (χ = 177.3°, t_χ = 0.22Å). When the TorS tower bundles of the apo and TMAO-bound complexes are superimposed, the CTDs of TorT' and TorT'' are rotated from the symmetric $TorT^T$ by 1.1° and 1.9° respectively, whereas the respect ive NTDs of TorT' and TorT'' are rotated 2.8° and 3.8° (Fig. 4C). Rotation axes are nearly parallel to the diad axis of the complex. The two apo TorT protomers are counter-rotated relative to $TorT^T$, whereby the cumulative deviation from symmetry is 6.6° for the NTDs and 2.8° for the CTDs. If TorT' is superimposed onto one $TorT^T$ protomer, both TorT'' domains must be rotated counterclockwise as viewed toward the membrane (Fig. 4C) to superimpose onto the other $TorT^T$ protomer.

The asymmetry that is evident in the apo TorT conformations propagates through the apo TorS protomers. After superposition of the apo and TMAO-bound tower bundles (Fig. 4D), the distal bundles of TorS' and TorS'' must each be rotated by ~3° for superpositions onto the corresponding bundles of $TorS^T$. Both rotations are in the same direction and about parallel axes nearly perpendicular to the molecular diad (Table S3C, Fig. 4E). These rotations swing the rest of TorS'/TorS'' relative to the tower bundle in a manner consistent with the interdomain moves of TorT' and TorT'' (Fig. 4C), the CTD-tower contact acting as a fulcrum. Finally, with the distal bundles so superimposed, the matching of proximal bundles from TorS' and TorS'' to corresponding $TorS^T$ bundles requires rotations of ~3° and ~8°, respect ively, about axes almost parallel to the molecular diad axis (Table S3D, Figs. 4C,E). Both rotations are in the same direction, but they add to a cumulative clockwise rotation of 5° from the apo to the TMAO-bound conformation, which is consistent with the transformation that superimposes the proximal TorS' and TorS'' bundles (χ = 185.0°, t_χ = -0.56Å).

Signal Transmission through the TorT-TorS complex

When TMAO binds to the TorT-TorS complex, it sends a signal through the length of the long TorS dimer, across the plasma membrane and on to the kinase domains; whereupon the phospho-relay cascade ensues. This signal transmission necessarily entails conformational change. Differences between the apo and TMAO-bound conformations are rather subtle, but the response to TMAO binding is concerted, directional and significant. Asymmetry in the disposition of apo-state TorT molecules (χ = 174.6° for NTDs) propagates through the left-handed distal bundles, which themselves are nearly symmetric (χ = 180.9°), to impart a counter rotation of the right-handed proximal bundles (χ = 185.0°). Ultimately, transmembrane signaling must involve relative displacements of helices α1 and α6 as these are the only elements that traverse the membrane. After superposition of the proximal domain of TorS'' onto the corresponding proximal domain of $TorS^T$ (the more similar pairing of the two, Table S3B), TorS' helices α1 and α6 are displaced by rotations of 7.9°

and 4.1°, resp ectively, and α1 moves upwards by 0.21Å whereas α6 moves downwards by 0.34Å for a cumulative piston-like shift of 0.55Å (Fig. S4A).

To examine the possible effect on signal transmission of interfacial contacts between proximal domains in the TorS dimer, we tested mutational variants at sites of contact using our β-galactosidase reporter assay. There is little conservation at these contacts, however, and we found little effect of the mutations tested (Table S2B). Since an accidentally mutant receptor having three residues deleted from helix α6 near the membrane interface is constitutively active (Jourlin et al., 1996), we also tested related insertions and deletions and systematic series of tryptophan and tyrosine shifts within α1 and α6 at both putative membrane interfaces. Nearly all gave perturbed responses, mainly partially constitutive activity (Table S2B), indicating a delicate control of signal transmission by the transmembrane helix bundle. Finally, we constructed several chimeric proteins having NarX or Tar sensor domains fused at various junctions to the TorS cytoplasmic domain and tested the activity of these chimeras. Similar chimeras between one sensor domain and an alternative cytoplasmic domain have been described (Ninfa, 2010), including a notably successful NarX-Tar fusion (Ward et al., 2002). In our case, one NarX-TorS chimera was found to be kinase-responsive to nitrate (Table S3D); others were insensitive to the appropriate ligand. The junctional transition is a very sensitive one.

Structural Dynamics and Formation Thermodynamics for TorT-TorS$_S$ Complexes

The apo and TMAO-bound differ in dynamic characteristics as well as in structural dispositions. Crystallographic B-factors provide a measure of atomic mobility, reflecting the dynamics within a structure. Atomic mobilities vary through the structures in differing ways for the two states (Figs. 5A,B). Most noticeably, the tower bundles and TorT subunits, particularly in CTD portions, are appreciably better ordered in the TMAO-bound state than when unligated (Fig. S5). In contrast, the apo-state structure is better ordered at the lower portions of the TorS distal bundles (e.g. α4-α5 loops) and at the inter-bundle junctions of α3 and α6 helices. Although the apo-state structure is structurally asymmetric, it is quasi-symmetric in atomic mobilities; similarities between the two halves are striking (Fig. 5A) despite substantial differences in lattice contacts.

The signaling complex for the TMAO-responsive histidine kinase receptor forms from the association of TMAO with TorT and TorS to an ultimate 2:2:2 stoichiometry. Dissection of this formation process is complicated by its many possible intermediates. Physiologically, the system is simplified since the TorS receptor is constitutively dimeric in the plasma membrane due to its dimeric cytoplasmic portions (Marina et al., 2005); however, isolated vpTorS$_S$ associates only relatively weakly into dimers (K_d = 282 μM; Moore and Hendrickson, 2009). Thus, in order to study the complex formation *in vitro* in a manner reflective of the *in vivo* situation, we designed a dimeric TorS$_S$-TorS$_S$ sensor construct having two TorS$_S$ sequences connected by a flexible 25-residue linker as fits the TorT-TorS$_S$ structures. We then first used sedimentation-equilibrium analytical ultracentrifugation (AUC) to study the thermodynamics of complex formation in the presence and absence of TMAO (Figs. 5C,D). In both cases, fittings to a (TorT)$_2$(TorS$_S$-TorS$_S$) model gave individual K_ds without significant differences, and so we report fittings constrained to be the same. The dissociation constants obtained without TMAO, $K_{d1} = K_{d2} = 1.79 \pm 0.26$ μM, are significantly higher than those, $K'_{d1} = K'_{d2} = 0.41 \pm 0.06$ μM, obtained in a saturating concentration of TMAO (10 mM). This greater energy of stabilization for the TMAO-complex correlates well with the decreased atomic mobility at the TorT-TorS$_S$ interactions in the TMAO-bound complex as compared to the apo complex (Figs. 5A,B).

Next, we used isothermal titration calorimetry (ITC) to study the thermodynamics of TMAO binding. Here, to assure compatibility with the AUC results, we combined TorT with the

$TorS_S$-$TorS_S$ construct, using concentrations sufficient for full complexation (Fig. 5E). The resulting ITC data were fit best by a two-site model for sequential binding at two independent sites: a high-affinity site with $K_d^{L1} = 1.36 \pm 0.064$ μM and a weaker second site with $K_d^{L2} = 121 \pm 4.7$ μM. Thus, TMAO binds to the TorT-TorS receptor with negative cooperativity. The thermodynamic separation into two binding sites is compatible with the structural distinction in the asymmetric apo-state complex. Which thermodynamic site corresponds to which structural site is less obvious, but the thermodynamic division of binding energy into enthalpic (ΔH) and entropic (-TΔS) contributions provides a clue. The high-affinity TMAO site stores a free energy of ΔG = -7.87 kcal/mol divided into enthalpic and entropic components of -6.29 and -1.58 kcal/mol, respectively, whereas the low-affinity site binding site has a free energy of -5.25 kcal/mol divided as -7.14 and +1.89 kcal/mol, respectively, into enthalpy and entropy. The apo TorT' and TorT" binding sites are very similar to one another and also to TMAO-bound $TorT^T$ (Figs. 3A-C) and TorT atomic mobilities are reduced generally upon TMAO binding (Figs. 5A,B), which would be expected to incur an entropic penalty. Whereas the binding to TorT' simply entails the addition of TMAO with displacement of one water molecule, the binding to TorT" requires that the essential βF-α5 loop must disorder. This disordering transition in TorT" is expected to be entropically favorable. Thus, the structures are compatible with identification of apo TorT" with the high affinity site and TorT' with the low affinity site.

From the combined AUC and ITC results, it is possible to construct the thermodynamic cycle for formation of the receptor complex and its binding of TMAO (Fig. 5F), inferring that TMAO binds to free vpTorT with energetics corresponding to $K_d = 73.6$ μM. This compares with the reported K_d of 150 μM for TMAO binding to ecTorT (Baraquet et al., 2006).

DISCUSSION

With this study we provide a comprehensive picture of the signaling sensor complex for the TMAO receptor. We find that TorT and the sensor portion of TorS interact directly, as was known (Baraquet et al., 2006), but now showing 2:2 stoichiometry. We also thoroughly characterize the thermodynamics for formation of TorT-$TorS_S$-TMAO complexes, and we describe crystal structures of TorT-$TorS_S$ complexes both with and without the TMAO or surrogate ligands. The apo and TMAO-bound complexes are superficially similar, but concerted conformational changes propagate through TorS from the distal TorT initiation sites upon TMAO binding down into the transmembrane helices for transmission to the phospho-relay cascade. The apo-state structure is markedly asymmetric but the TMAO-bound structure is symmetric. Our mutational analyses validate the essentiality of binding-site and gating-loop structures for cellular function of intact TorT-TorS receptor complexes, and a NarX-TorS chimera ties the TorS system mechanistically to other histidine kinase and chemotaxis receptor systems.

Negative Cooperativity from Asymmetric Empty Sites

TMAO binds to the TorT-$TorS_S$ heterotetramer with two markedly different binding affinities, in a binding profile (Fig. 5E) having the hallmarks of negative cooperativity (Koshland, 1996). The aspartate receptor Tar (Yeh et al., 1996) is a classic negatively cooperative protein, and the EGF receptor (Alvarado et al., 2010; Macdonald and Pike, 2008) is a more recently proven example. The conventional explanation for the phenomenon, demonstrated in all previous cases where structures are known, has it that ligand binding to one site in a symmetric protein induces conformational changes that break symmetry and reduce affinity at subsequent sites. Here, the explanation is exceptional and opposite. The apo-state TorT-$TorS_S$ structure is intrinsically asymmetric with two distinct TMAO-binding sites; symmetry is achieved when TMAO binds to both sites, but asymmetry

must be reinforced with binding only to the high-affinity site. While binding to the first TorT site might affect the conformation and affinity at the second site, the observations do not require such a model. The essential characteristic of negative cooperativity that remains is a symmetry/asymmetry transition; however, whereas ligand binding classically breaks symmetry, TMAO binding to TorT/TorS$_S$ generates symmetry.

Which thermodynamic site of TorT/TorS corresponds to which structural site? Structurally, TMAO binds into a highly conserved site, and mutations at five of six ligand-contacting residues entirely abolish the cellular response to TMAO (Fig. 3D). A second highly conserved TorT feature is the gating βF-α5 loop (GPXXXGG), which is also highly sensitive to mutation (Fig. 3E). The gating loop is disordered in the TMAO-bound structure and in apo TorT', but it is ordered in apo TorT" and must be displaced to permit TMAO to bind. Otherwise, the two apo sites are very similar, both to one another and to TMAO-bound TorT^T. Qualitatively, the conformations are compatible with similarities in enthalpic contributions for TMAO binding to the two sites. The substantial reduction in atomic mobility that accompanies TMAO binding (Figs. 5A,B) is expected to produce an entropic penalty. This penalty is evident at the low-affinity site, whereas the required disordering of the gating loop in TorT" is compatible with a compensating favorable entropic contribution to TMAO binding at the high-affinity site. Thus, we see a structural basis for this altenative kind of negative cooperativity.

Relevance for the Physiological TMAO Receptor

The heterotetrameric TorT-TorS$_S$ complex that we study here *in vitro* (and in crystals) is only part of the intact receptor system, extracted from its natural physiological context. Nevertheless, given values from our thermodynamic cycle (Fig. 5F) and our *in vivo* mutational tests, this picture of the sensor complex seems likely to be physiologically relevant. Since the cytoplasmic and transmembrane portions of histidine kinase receptors are intrinsically dimeric (Gordeliy et al., 2002; Marina et al., 2005), the periplasmic sensor domain portions are necessarily dimeric as well. Thus, the relatively weak TorS$_S$ self associations (Moore and Hendrickson, 2009) will be greatly potentiated in intact receptors, as is also true in linker-fused TorS$_S$-TorS$_S$ dimers used in our thermodynamic studies. Unless TorT were at exceptionally low abundance, its association into signaling complexes with TorS will predominate, whether in presence of TMAO or not. This is so both for *V. parahaemolyticus* with TorT-TorS K$_d$s in the vicinity of 1 μM and, even more so, for *E. coli* (K$_d$ ~10 nM (Baraquet et al., 2006)). Thus, the sensor complexes are mainly preformed. Based on our reporter assays, the cellular response is not evident until the TMAO concentration in the medium is above 1 mM, which suggests that responses likely require transition to the doubly occupied, symmetric TMAO-bound state. Quite possibly, the negative cooperativity is tuned to assure that *torCAD* genes are turned on only when TMAO supplies are adequate to support respiration.

The apo and TMAO-bound structures are sufficiently similar (Figs. 3A-C, 4D,E) that the influence of lattice contacts could be a concern; however, multiple lines of evidence support the functional relevance of these structures. First, those crystallization conditions identified in the presence of TMAO were unique from those identified without TMAO, except for the ones that ultimately yielded the isopropanol-bound structure. Moreover, the lattice of the apo structure is incompatible with the TMAO-bound state; crystals are destroyed when soaked in TMAO concentrations greater than 1 μM and the lattice changes when soaked for several seconds at 1 μM TMAO. Second, binding thermodynamics agree with structural distinctions. The reduction of atomic mobility in TorT and distal TorS upon TMAO binding (Figs. 5A,B) is compatible with the higher TorT-TorS affinity when in presence of TMAO (Figs. 5C,D); and, most tellingly, TMAO binds with two distinct thermodynamic signatures (Fig. 5E) that can be rationalized with features at two binding sites in the apo structure,

including the ordered gating loop in one, as compared to the TMAO-bound structure (Figs. 3A-C). Finally, the conformational differences between the apo and TMAO-bound structures involve concerted twists and counter twists that are incompatible with effects that can be imagined from the lattice contacts in these crystals.

Comparative Architecture of Histidine Kinase Receptor Complexes

In typical two component systems, the ligand binds directly to the sensor domain to effect signal transduction through the receptor. In some others, as here for TorS, the ligand-receptor interaction is indirect, mediated by a PBP protein. Commonly, ligand binding to the PBP is required for PBP-sensor interaction (e.g. in the BctC-BctE system for citrate signaling (Antoine et al., 2005) and in the MBP-Tar chemotaxis system for maltose signaling (Zhang et al., 1999)). ternatively, as in the CBP-ChiS system for chitin signaling (Li and Roseman, 2004), ligand binding dissociates the PDB to release inhibition. Finally, here in the TorT-TorS system as in the LuxP-LuxQ system for AI-2 signaling (Neiditch et al., 2006), the PBP binds to the sensor domain both with and without its ligand.

The only previous structures of PBP-sensor complexes are those of LuxP-$LuxQ_S$. The known apo structure is a 1:1 complex (Neiditch et al., 2005; Neiditch et al., 2006), but the overall architecture of LuxP-$LuxQ_S$ complexed with AI-2 (Neiditch et al., 2005; Neiditch et al., 2006) parallels TorT-$TorS_S$. Both complexes are 2:2 heterotetramers with the PBP bound to the distal domains of both sensor protomers. Also, both sensor domains are inserted repeats; however, whereas $TorS_S$ is an all-α protein, $LuxQ_S$ comprises two α+β PDC domains (Zhang and Hendrickson, 2010). VirA, another all-α sensor protein that acts through a PBP (sugar binding ChvE), is also dimeric (Nair et al., 2011).

Signal Initiation in TorT and Related Co-Receptors or Receptors

Signaling through the TorT/TorS/TorR receptor system begins with the binding of TMAO to TorT, and signal transmission is fueled by the energy from that binding, totaling 13.1 kcal/mol of tetramers. The conformational changes that occur within TorT subunits are relatively slight, with interdomain closure by only 2.6° for TorT" relative to $TorT^T$ and actually an opening (2.3°) for TorT', but these shifts lead to concerted changes through the length of the TorS dimer. The only other PBP co-receptor for a histidine kinase receptor with known structures, LuxP, undergoes much greater hinge bending; with an interdomain closure of 29° upon AI-2 binding (Neiditch et al., 2006); this is more typical of ligand binding to PBPs (Quiocho and Ledvina, 1996). The constitutively closed arrangement in TorT is not unique, however. PBP sensor domains from the histidine kinase receptors BvgS of *Bordetella pertussis* (Herrou et al., 2010) and gene product GSU2755 from *Geobacter sulfurreducens* (Cheung et al., 2009) reveal unliganded structures in a closed state. Neither has an identified ligand.

Signal Transmission through TorS and Related Receptors

Exactly how the signal initiated by TMAO binding to TorT is transmitted through TorS to its phospho-relay cascade remains unclear, but comparisons of TorS to other receptors give hints. The proximal domain of $TorS_S$ is similar in structure to the sensor domains of NarX and Tar (Moore and Hendrickson, 2009), and all three make similar dimers (Figs. S3B,C). Furthermore, comparisons of natural NarX, TorS and Tar signaling with the chimeric (sensor-cytoplasmic) receptors NarX-TorS (this work) and NarX-Tar (Ward et al., 2002) imply a shared mode of signaling. Nitrate binding to Tar and TMAO binding to TorT/TorS both yield kinase activity and aspartate binding to Tar generates phosphatase activity, while nitrate binding to either the NarX-TorS or NarX-Tar chimera produces kinase activity. The very existence of active chimeras suggests commonality in signaling, but structure-function analyses further mechanistic insight.

The chemoreceptor Tar is the best studied of these all-α sensors. Aspartate binding to half of the sites produces an asymmetric Tar dimer and induces a piston-like downward displacement of helix α4 in one of the protomers (Biemann and Koshland, 1994; Chervitz and Falke, 1996), and this aspartate binding results in an attractant response due to dephosphorylation (Jin and Inouye, 1993). In contrast, nitrate binding by NarX is thought to induce an upward displacement of helix α4 (Cheung and Hendrickson, 2009; Falke and Erbse, 2009); and nitrate binding in NarX promotes phosphorylation (Cavicchioli et al., 1996; Williams and Stewart, 1997). Consistent with the opposite directionality of displacements and activity in Tar and NarX function, the NarX-Tar fusion generates a kinase-based repulsive response to nitrate (Ward et al., 2002). The kinase responses of both TorT/TorS to TMAO (Jourlin et al., 1997) and NarX-TorS to nitrate is compelling evidence of a similar mechanism in TorS as in Tar and NarX; however, conformational changes in seen here in TorS are even more subtle than those described for Tar and NarX.

We expect that even such subtle changes can exert a controlling influence on activity given the long lever arm from TorT through TorS and into the cytoplasmic dimerization domain. We observed previously that the kinase domain latch can be released readily by conservative mutation (Marina et al., 2005), and we suggest that torques applied by TMAO binding in the TorT/TorS system might similarly unlatch the kinase for histidine phosphorylation.

Asymmetry vs. Symmetry in Histidine Kinase Signaling

The ligand-bound state of a histidine kinase sensor generates kinase activity for many receptors and phosphatase activity for others. Where characterized, the apo state presents the ternative activity constitutively. Thus, histidine kinases differ qualitatively from receptor tyrosine kinases where ligand binding produces an ‘on’ state that needs an exogenous phophatase to be turned off; histidine kinase receptors can be described better as being controlled by ‘either-or’ switches rather than by ‘on-off’ switches.

A number of histidine kinase sensor-domain structures are known, but the TorT-TorS$_S$ system is the first with structures for both the apo and ligand-bound states of the dimeric sensor complex. Structurally, the TorT-TorS$_S$ complex in the apo, phosphatase-equivalent state is asymmetric, whereas the TMAO-bound and kinase-equivalent state is symmetric. To put this observation in context, we looked at the known structures of biologically relevant sensor domain dimers. We found that all complexes in the kinase-equivalent state are symmetric and that all in the phosphatase-equivalent state are asymmetric (Table 2). A somewhat equivocal case concerns the red-light receptor BphP (Yang et al., 2008; Yang et al., 2009). Here, one dimeric structure is an asymmetric complex in the phosphatase-equivalent Pr (dark) state; the other is a symmetric structure of a mutant that crystallized as a mix of Pr and kinase-equivalent Pfr states.

The association of kinase activity with asymmetry and phosphatase activity with asymmetry is also evident in the Tar chemotactic receptor (Yeh et al., 1996). Furthering the parallel, both Tar and TorT/TorS are negatively cooperative. Moreover, the correspondences of structural knowledge with activity responses from chimeric receptors, including our NarX-TorS chimera, all identify kinase activity with the symmetric state and phosphatase activity with the asymmetric state. Ligand binding seems to control the symmetry of the complex, thereby positioning the ‘either-or’ activity switch. We speculate that the observed subtlety of ligand-elicted conformational changes in TorT-TorS$_S$ and Tar arises because the same cytoplasmic domains perform the alternative enzymatic reactions. Many questions remain. In particular, there is the puzzle of how structural changes induced in the sensor are transmitted through the membrane and cytoplasmic domains to control kinase and phosphatase activity.

EXPERIMENTAL PROCEDURES

Cloning, Expression and Purification for Biophysical Studies

The isolated vpTorS$_S$ sensor domain, GSGS-TorS(51-323), was produced in *E. coli* as described previously (Moore and Hendrickson, 2009). An expression plasmid for vpTorT (residues 29-329) was cloned from genomic DNA of *V. parahaemolyticus.* Purified GSGS-TorT(29-329) produced from *E. coli* was able to bind vpTorS$_S$ and the complex was purified by size exclusion chromatography (SEC).

A vpTorS$_S$-TorS$_S$ dimer was produced in E. coli from a plasmid that would fuse two copies of vpTorS$_S$ (51-323) via a flexible linker [LN(SG)$_{10}$A$_3$]. Purified TorS$_S$-TorS$_S$ was used with TorT for AUC studies and complexes of TorS$_S$-TorS$_S$-(TorT)$_2$ were purified by SEC for ITC measurements.

Crystallization, Diffraction Measurements and Structure Determination

Crystals of three different forms were grown at 4°C by hanging drop vapor diffusion, with and without TMAO, stabilized in cryoprotective buffers, and frozen to 110 K for data collection at NSLS beamline X4C or at APS beamline 14-BM-C. First, the structure of the TorT-TorS$_S$ heterotetramer bound to isopropanol was solved from a 4λ selenomethionyl MAD experiment. This structure was refined and then used to determine structures of the TMAO-bound and apo structures by molecular replacement.

Analytical Ultracentrifugation

The complex of vpTorT and vpTorS$_S$-TorS$_S$ was formed at 2:1 stoichiometery and purified by SEC to remove unreactive digested TorT, and this preparation at ~1.5 mg/mL was centrifuged at 20°C in the absence or presence of 10 mM TMAO to equilibrium at 10K, 13K and 16K rpm in a Beckman XLI centrifuge. Data were analyzed using HeteroAnalysis.

Isothermal Titration Calorimetry

ITC measurements were carried out at 20°C on a VP–I TC microcalorimeter (GEHealthcare, Microcal, Northhampton, MA) with 30 μM purified vpTorS$_S$-TorS$_S$(TorT)$_2$ complex in the cell after a series of 5 μL injections of 1.2 mM TMAO in the syringe. Data were analyzed by Origin 7.0.

Cell Strains and Cloning for Analyses of Cellular Activity

Bacterial strains for use in β-galactosidase assays were generated from strain N7723 (genotype N99 *lacZX*A21) generously provided by the Gottesman laboratory. Ultimately, the *torS-torT* operon was deleted, and the *pcnB* gene was removed to control against plasmid copy proliferation (Jourlin et al., 1997), to yield strain N7723ΔTS-pCN. Then, a plasmid, called pCAD-*lacZ*/TS, was generated to incorporate the *E. coli torT-torS* locus and to place a *lacZ* gene under regulatory control of the *E.coli torCAD* operon. TorT/TorS mutations were made in pCAD-*lacZ*/TS by QuikChange (Stratagene). To generate Tar and NarX chimeras, we used conserved mutations to engineer suitable restriction sites into pCAD-*lacZ*/TS to make the chimeric swaps. Various pCAD-*lacZ*/TS plasmids were introduced into N7723ΔTS-pCN for functional assays.

β-Galactosidase Assay

All strains were grown overnight in appropriate media at 37°C. Following 1:1000 dilution into 5 mL tubes filled with media and the appropriate concentration of TMAO (nitrate or aspartate for NarX or Tar chimeras, respectively), the tubes were capped to leave little air,

and then incubated for five hours at 37°C. Activity was mea sured using a β-galactosidase assay kit (Pierce Biotechnology).

Supplementary Material

Refer to Web version on PubMed Central for supplementary material.

Acknowledgments

We thank Joe Lidestri, Randy Abramowitz, and John Schwanof for help with synchrotron data collection at NSLS X4C and the staff at BioCARS for help at APS 14-BM-C; Goran Ahlsen for help analyzing the AUC experiments; Ewa-Folta Stogniew with the Keck Biophysics Resource at Yale University School of Medicine for performing the ITC experiments; and Christal Vitiello and Max Gottesman for help with cell-line constructions. This work was supported in part by NIH grant GM34102. Beamline X4C of the National Synchrotron Light Source (NSLS) at Brookhaven National Laboratory, a DOE facility, is supported by the New York Structural Biology Center.

References

Alvarado D, Klein DE, Lemmon MA. Structural basis for negative cooperativity in growth factor binding to an EGF receptor. Cell. 2010; 142:568–579. [PubMed: 20723758]

Ansaldi M, Jourlin-Castelli C, Lepelletier M, Theraulaz L, Mejéan V. Rapid dephosphorylation of the TorR response regulator by the TorS unorthodox sensor in *Escherichia coli*. J Bacteriol. 2001; 183:2691–2695. [PubMed: 11274133]

Ansaldi M, Theraulaz L, Baraquet C, Panis G, Mejéan V. Aerobic TMAO respiration in *Escherichia coli*. Mol Microbiol. 2007; 66:484–494. [PubMed: 17850256]

Antoine R, Huvent I, Chemlal K, Deray I, Raze D, Locht C, Jacob-Dubuisson F. The periplasmic binding protein of a tripartite tricarboxylate transporter is involved in signal transduction. J Mol Biol. 2005; 351:799–809. [PubMed: 16045930]

Baraquet C, Theraulaz L, Guiral M, Lafitte D, Mejéan V, Jourlin-Castelli C. TorT, a member of a new periplasmic binding protein family, triggers induction of the Tor respiratory system upon trimethylamine N-oxide electron-acceptor binding in *Escherichia coli*. J Biol Chem. 2006; 281:38189–38199. [PubMed: 17040909]

Barrett EL, Kwan HS. Bacterial reduction of trimethylamine oxide Annu. Rev Microbiol. 1985; 39:131–149.

Bhoo SH, Davis SJ, Walker J, Karniol B, Vierstra RD. Bacteriophytochromes are photochromic histidine kinases using a biliverdin chromophore. Nature. 2001; 414:776–779. [PubMed: 11742406]

Biemann HP, Koshland DE Jr. Aspartate receptors of *Escherichia coli* and *Salmonella typhimurium* bind ligand with negative and half-of-the-sites cooperativity. Biochemistry. 1994; 33:629–634. [PubMed: 8292590]

Björkman AJ, Mowbray SL. Multiple open forms of ribose-binding protein trace the path of its conformational change. J Mol Biol. 1998; 279:651–664. [PubMed: 9641984]

Bott M, Meyer M, Dimroth P. Regulation of anaerobic citrate metabolism in *Klebsiella pneumoniae*. Mol Microbiol. 1995; 18:533–546. [PubMed: 8748036]

Cavicchioli R, Chiang RC, Kalman LV, Gunsalus RP. Role of the periplasmic domain of the *Escherichia coli* NarX sensor-transmitter protein in nitrate-dependent signal transduction and gene regulation. Mol Microbiol. 1996; 21:901–911. [PubMed: 8885262]

Chervitz SA, Falke JJ. Molecular mechanism of transmembrane signaling by the aspartate receptor: a model. Proc Natl Acad Sci USA. 1996; 93:2545–2550. [PubMed: 8637911]

Cheung J, Bingman CA, Reyngold M, Hendrickson WA, Waldburger CD. Crystal structure of a functional dimer of the PhoQ sensor domain. J Biol Chem. 2008; 283:13762–13770. [PubMed: 18348979]

Cheung J, Hendrickson WA. Crystal structures of C4-dicarboxylate ligand complexes with sensor domains of histidine kinases DcuS and DctB. J Biol Chem. 2008; 283:30256–30265. [PubMed: 18701447]

Cheung J, Hendrickson WA. Structural analysis of ligand stimulation of the histidine kinase NarX. Structure. 2009; 17:190–201. [PubMed: 19217390]

Cheung J, Hendrickson WA. Sensor domains of two-component regulatory systems. Curr Opin Microbiol. 2010; 13:116–123. [PubMed: 20223701]

Cheung J, Le-Khac M, Hendrickson WA. Crystal structure of a histidine kinase sensor domain with similarity to periplasmic binding proteins. Proteins. 2009; 77:235–241. [PubMed: 19544572]

Falke JJ, Erbse AH. The piston rises again. Structure. 2009; 17:1149–1151. [PubMed: 19748334]

Freeman JA, Bassler BL. A genetic analysis of the function of LuxO, a two-component response regulator involved in quorum sensing in *Vibrio harveyi*. Mol Microbiol. 1999; 31:665–677. [PubMed: 10027982]

Gao R, Stock AM. Biological insights from structures of two-component proteins. Annu Rev Microbiol. 2009; 63:133–154. [PubMed: 19575571]

Gon S, Giudici-Orticoni MT, Mejéan V, Iobbi-Nivol C. Electron transfer and binding of the c-type cytochrome TorC to the trimethylamine N-oxide reductase in *Escherichia coli*. J Biol Chem. 2001; 276:11545–11551. [PubMed: 11056172]

Gordeliy VI, Labahn J, Moukhametzianov R, Efremov R, Granzin J, Schlesinger R, Buldt G, Savopol T, Scheidig AJ, Klare JP, et al. Molecular basis of transmembrane signalling by sensory rhodopsin II-transducer complex. Nature. 2002; 419:484–487. [PubMed: 12368857]

Herrou J, Bompard C, Wintjens R, Dupre E, Willery E, Villeret V, Locht C, Antoine R, Jacob-Dubuisson F. Periplasmic domain of the sensor-kinase BvgS reveals a new paradigm for the Venus flytrap mechanism. Proc Natl Acad Sci USA. 2010; 107:17351–17355. [PubMed: 20855615]

Hollenstein K, Frei DC, Locher KP. Structure of an ABC transporter in complex with its binding protein. Nature. 2007; 446:213–216. [PubMed: 17322901]

Hulko M, Berndt F, Gruber M, Linder JU, Truffault V, Schultz A, Martin J, Schultz JE, Lupas AN, Coles M. The HAMP domain structure implies helix rotation in transmembrane signaling. Cell. 2006; 126:929–940. [PubMed: 16959572]

Hvorup RN, Goetz BA, Niederer M, Hollenstein K, Perozo E, Locher KP. Asymmetry in the structure of the ABC transporter-binding protein complex BtuCD-BtuF. Science. 2007; 317:1387–1390. [PubMed: 17673622]

Janausch IG, Garcia-Moreno I, Unden G. Function of DcuS from *Escherichia coli* as a fumarate-stimulated histidine protein kinase in vitro. J Biol Chem. 2002; 277:39809–39814. [PubMed: 12167640]

Jin T, Inouye M. Ligand binding to the receptor domain regulates the ratio of kinase to phosphatase activities of the signaling domain of the hybrid *Escherichia coli* transmembrane receptor, Taz1. J Mol Biol. 1993; 232:484–492. [PubMed: 8393937]

Jourlin C, Ansaldi M, Mejéan V. Transphosphorylation of the TorR response regulator requires the three phosphorylation sites of the TorS unorthodox sensor in *Escherichia coli*. J Mol Biol. 1997; 267:770–777. [PubMed: 9135110]

Jourlin C, Bengrine A, Chippaux M, Méjean V. An unorthodox sensor protein (TorS) mediates the induction of the tor structural genes in response to trimethylamine N-oxide in *Escherichia coli*. Mol Microbiol. 1996; 20:1297–1306. [PubMed: 8809780]

Kim C, Jackson M, Lux R, Khan S. Determinants of chemotactic signal amplification in *Escherichia coli*. J Mol Biol. 2001; 307:119–135. [PubMed: 11243808]

Koshland DE Jr. The structural basis of negative cooperativity: receptors and enzymes. Curr Opin Struct Biol. 1996; 6:757–761. [PubMed: 8994875]

Li X, Roseman S. The chitinolytic cascade in Vibrios is regulated by chitin oligosaccharides and a two-component chitin catabolic sensor/kinase. Proc Natl Acad Sci USA. 2004; 101:627–631. [PubMed: 14699052]

Macdonald JL, Pike LJ. Heterogeneity in EGF-binding affinities arises from negative cooperativity in an aggregating system. Proc Natl Acad Sci USA. 2008; 105:112–117. [PubMed: 18165319]

Marina A, Waldburger CD, Hendrickson WA. Structure of the entire cytoplasmic portion of a sensor histidine-kinase protein. EMBO J. 2005; 24:4247–4259. [PubMed: 16319927]

Mejéan V, Iobbi-Nivol C, Lepelletier M, Giordano G, Chippaux M, Pascal MC. TMAO anaerobic respiration in *Escherichia coli*: involvement of the tor operon. Mol Microbiol. 1994; 11:1169–1179. [PubMed: 8022286]

Milburn MV, Prive GG, Milligan DL, Scott WG, Yeh J, Jancarik J, Koshland DE Jr, Kim SH. Three-dimensional structures of the ligand-binding domain of the bacterial aspartate receptor with and without a ligand. Science. 1991; 254:1342–1347. [PubMed: 1660187]

Moore JO, Hendrickson WA. Structural analysis of sensor domains from the TMAO-responsive histidine kinase receptor TorS. Structure. 2009; 17:1195–1204. [PubMed: 19748340]

Nair GR, Lai X, Wise AA, Rhee BW, Jacobs M, Binns AN. The VirA sensor kinase of *Agrobacterium tumefaciens*: the integrity of the periplasmic domain is critical for optimal coordination of virulence signal response. J Bacteriol. 2011; 193:1436–1448. [PubMed: 21216996]

Neiditch MB, Federle MJ, Miller ST, Bassler BL, Hughson FM. Regulation of LuxPQ receptor activity by the quorum-sensing signal autoinducer-2. Mol Cell. 2005; 18:507–518. [PubMed: 15916958]

Neiditch MB, Federle MJ, Pompeani AJ, Kelly RC, Swem DL, Jeffrey PD, Bassler BL, Hughson FM. Ligand-induced asymmetry in histidine sensor kinase complex regulates quorum sensing. Cell. 2006; 126:1095–1108. [PubMed: 16990134]

Ninfa AJ. Use of two-component signal transduction systems in the construction of synthetic genetic networks. Curr Opin Microbiol. 2010; 13:240–245. [PubMed: 20149718]

Ninfa EG, Stock A, Mowbray S, Stock J. Reconstitution of the bacterial chemotaxis signal transduction system from purified components. J Biol Chem. 1991; 266:9764–9770. [PubMed: 1851755]

Oldham ML, Khare D, Quiocho FA, Davidson AL, Chen J. Crystal structure of a catalytic intermediate of the maltose transporter. Nature. 2007; 450:515–521. [PubMed: 18033289]

Quiocho FA, Ledvina PS. Atomic structure and specificity of bacterial periplasmic receptors for active transport and chemotaxis: variation of common themes. Mol Microbiol. 1996; 20:17–25. [PubMed: 8861200]

Sevvana M, Vijayan V, Zweckstetter M, Reinelt S, Madden DR, Herbst-Irmer R, Sheldrick GM, Bott M, Griesinger C, Becker S. A ligand-induced switch in the periplasmic domain of sensor histidine kinase CitA. J Mol Biol. 2008; 377:512–523. [PubMed: 18258261]

Simon G, Jourlin C, Ansaldi M, Pascal MC, Chippaux M, Mejéan V. Binding of the TorR regulator to cis-acting direct repeats activates tor operon expression. Mol Microbiol. 1995; 17:971–980. [PubMed: 8596446]

Simon G, Mejéan V, Jourlin C, Chippaux M, Pascal MC. The TorR gene of *Escherichia coli* encodes a response regulator protein involved in the expression of the trimethylamine N-oxide reductase genes. J Bacteriol. 1994; 176:5601–5606. [PubMed: 8083154]

Stewart RC. Protein histidine kinases: assembly of active sites and their regulation in signaling pathways. Curr Opin Microbiol. 2010; 13:133–141. [PubMed: 20117042]

Ward SM, Delgado A, Gunsalus RP, Manson MD. A NarX-Tar chimera mediates repellent chemotaxis to nitrate and nitrite. Mol Microbiol. 2002; 44:709–719. [PubMed: 11994152]

Williams SB, Stewart V. Discrimination between structurally related ligands nitrate and nitrite controls autokinase activity of the NarX transmembrane signal transducer of Escherichia coli K-12. Mol Microbiol. 1997; 26:911–925. [PubMed: 9426129]

Wolanin PM, Thomason PA, Stock JB. Histidine protein kinases: key signal transducers outside the animal kingdom. Genome Biol. 2002; 3 REVIEWS3013.

Yang X, Kuk J, Moffat K. Crystal structure of *Pseudomonas aeruginosa* bacteriophytochrome: photoconversion and signal transduction. Proc Natl Acad Sci USA. 2008; 105:14715–14720. [PubMed: 18799746]

Yang X, Kuk J, Moffat K. Conformational differences between the Pfr and Pr states in *Pseudomonas aeruginosa* bacteriophytochrome. Proc Natl Acad Sci USA. 2009; 106:15639–15644. [PubMed: 19720999]

Yeh JI, Biemann HP, Pandit J, Koshland DE, Kim SH. The three-dimensional structure of the ligand-binding domain of a wild-type bacterial chemotaxis receptor. Structural comparison to the cross-

linked mutant forms and conformational changes upon ligand binding. J Biol Chem. 1993; 268:9787–9792. [PubMed: 8486661]

Yeh JI, Biemann HP, Prive GG, Pandit J, Koshland DE Jr, Kim SH. High-resolution structures of the ligand binding domain of the wild-type bacterial aspartate receptor. J Mol Biol. 1996; 262:186–201. [PubMed: 8831788]

Zhang Y, Gardina PJ, Kuebler AS, Kang HS, Christopher JA, Manson MD. Model of maltose-binding protein/chemoreceptor complex supports intrasubunit signaling mechanism. Proc Natl Acad Sci USA. 1999; 96:939–944. [PubMed: 9927672]

Zhang Z, Hendrickson WA. Structural characterization of the predominant family oof histidine kinase sensor domains. J Mol Biol. 2010; 400:335–353. [PubMed: 20435045]

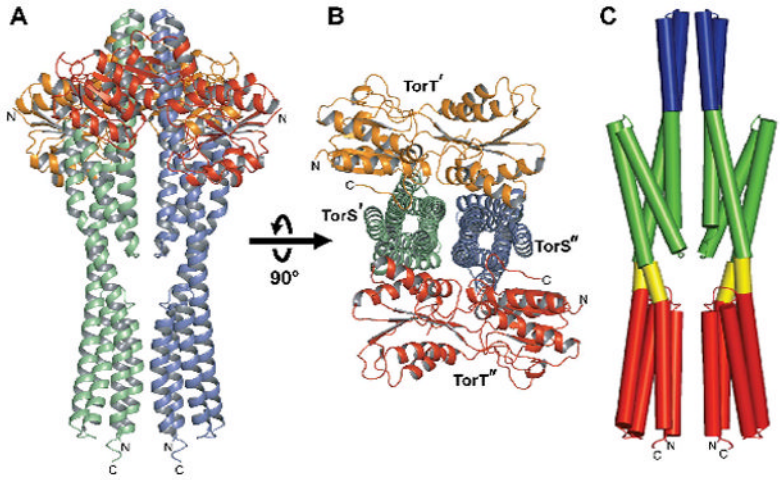

Figure 1. Structure of the TorT-TorS$_S$ Complex

(A) Ribbon diagram of the TMAO-bound vpTorT-vpTorS$_S$ complex. The molecular diad axis is vertical and the orientation would have the plasma membrane at the bottom. TorT protomers are colored orange and red; TorS$_S$ protomers are colored green and blue.

(B) Ribbon diagram of the complex viewed down diad axis, into the membrane, after being rotated 90° as indicated. Coloring is as in A.

(C) Cylinder diagram of the vpTorS$_S$ dimer. The orientation is as in a. The coloring code is tower bundle (blue), distal bundles (green), interbundle couplers (yellow), and proximal bundles (red).

See also Figure S2.

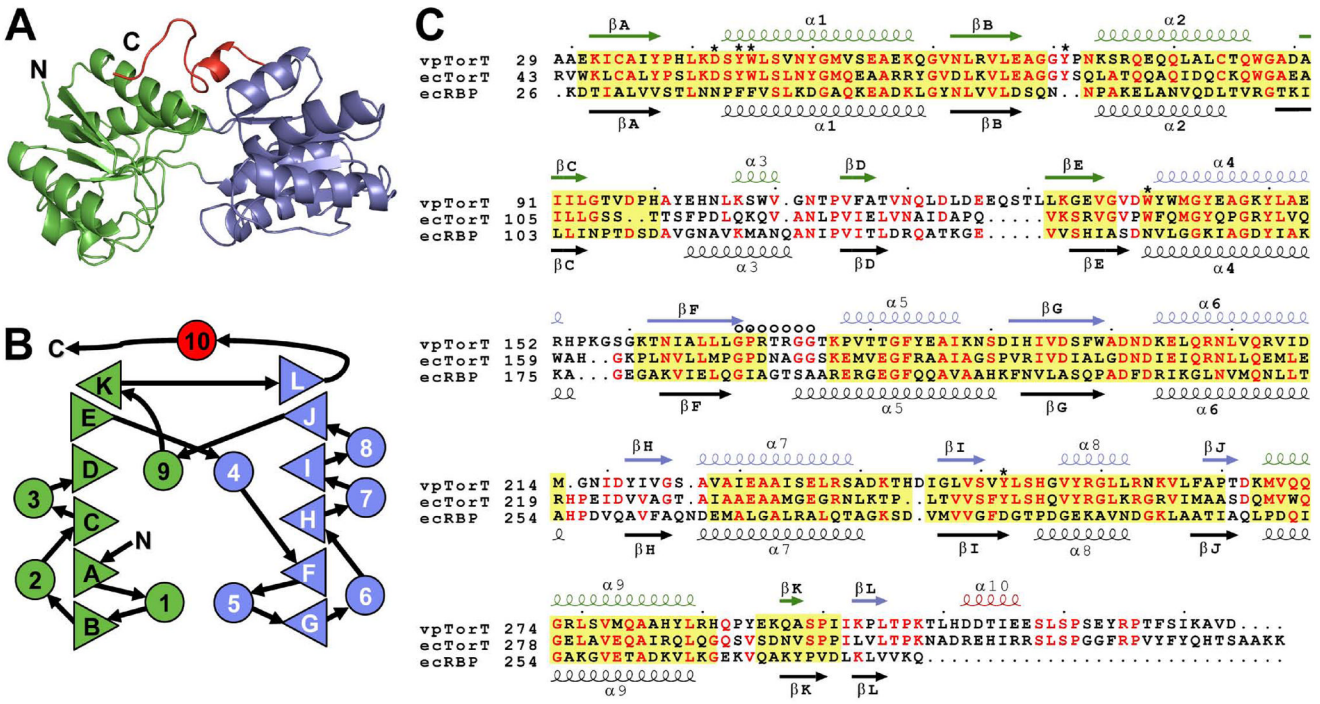

Figure 2. Structure-based TorT Sequence Alignments

(A) Ribbon diagram of the vpTorT" structure, which uniquely includes a fully ordered βF-α5 loop. Coloring is by domain: N-terminal domain, green; C-terminal domain, blue; C-terminal extension, red.

(B) Topology diagram of vpTorT. Triangles represent β strands and circles represent α helices. Rightward- and leftward-facing triangles are for strands going into and coming out from the page, respectively. Color coding of these elements is as in A.

(C) Structure-based sequence alignment. Amino acid sequences of *V. parahaemalyticus* TorT (vpTorT), *E. coli* TorT (ecTorT), and *E. coli* ribose binding protein (ecRBP) are aligned based on structural superpositions of vpTorT and ecRBP structures and numbered accordingly. Secondary structure elements are symbolized and labeled above and below the respective sequences. Conserved residues are shown in red and structurally aligned regions where at least three contiguous Cα positions of ecRBP are within 3.0Å of vpTorT^{T}, domain by domain, are shaded yellow. Residues that contact TMAO in TorT^{T} and the βF-α5 loop are indicated by * and ^{O}, respectively.

See also Figure S3.

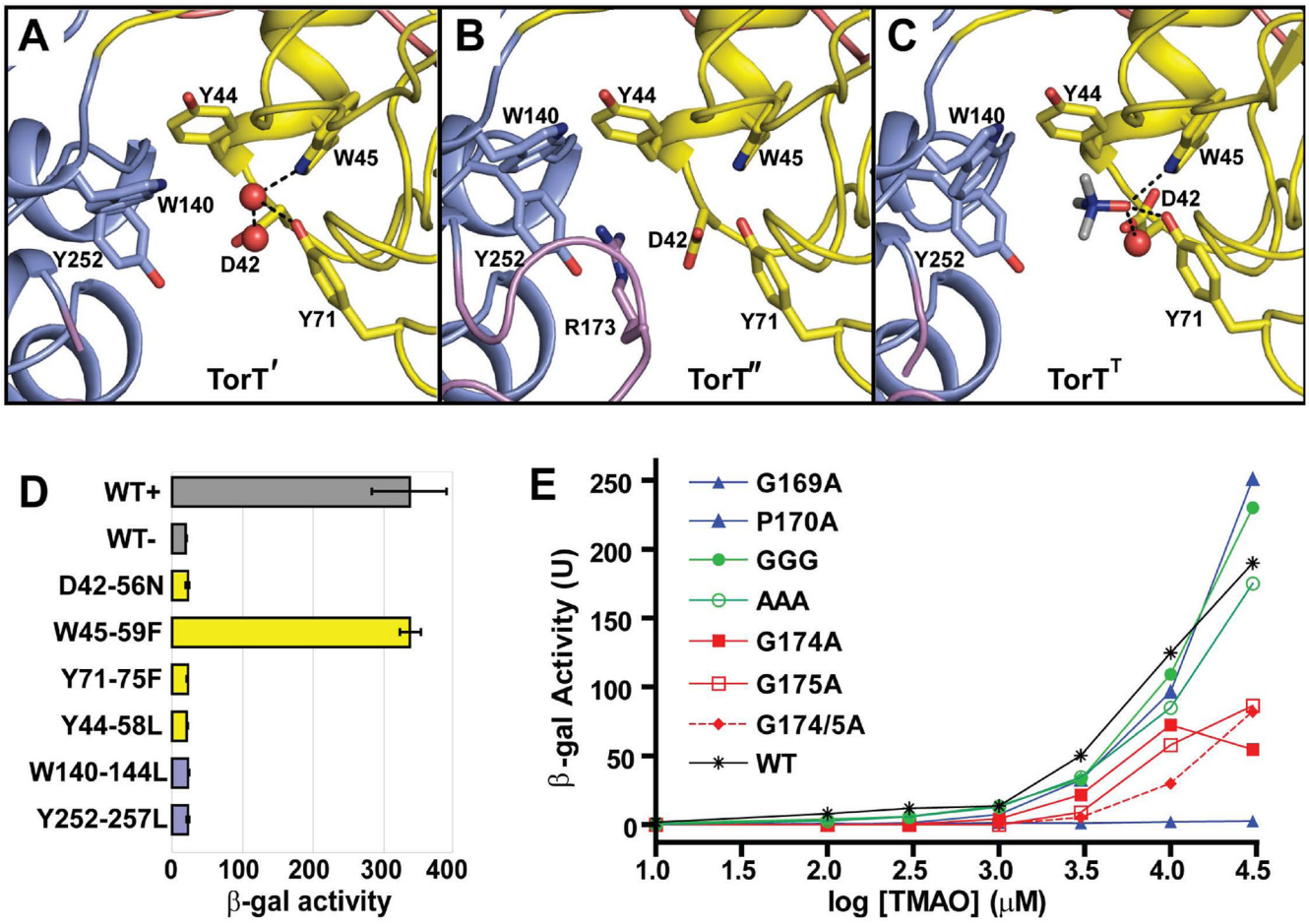

Figure 3. TMAO Binding Site and Mutational Analysis

(A-C) Ribbon diagrams of the TMAO binding site TorT', TorT" and TorT^T, respectively. The side chains of Asp42, Tyr44, Trp45, Tyr71, Trp140 and Tyr252 are identified in each. Arg173 is also labeled in TorT". Water molecules in the binding pockets of TorT' and TorT^T are shown as red spheres. The NTD and CTD are colored yellow and blue, respectively, and ordered portions of the βF-α5 loops are colored magenta.

(D) β-Galactosidase activity of binding pocket mutants. Each culture was grown in the presence of 10 mM TMAO, except for WT-, which was grown in the absence of TMAO. Each mutant is labeled such that the vpTorT residue is first followed by the corresponding residue number in *E. coli* and the resulting mutation. The wild type (WT) results are shown in gray; mutations of NTD and CTD residues are in yellow and blue, respectively.

(E) β-Galactosidase activity of βF-α5 mutants at a series of TMAO concentrations. Wild type is in black (* T-S), mutations of the N-terminal glycine or proline residues are in blue, mutations of the three intervening residues into glycine (GGG) or alanine (AAA) are in green, and mutations of the C-terminal glycine residues are in red. Cited residue numbers are those from vpTorT whereas those for this segment in ecTorT are 5 greater, e.g. vpP170 becomes ecP175.

See also Table S2.

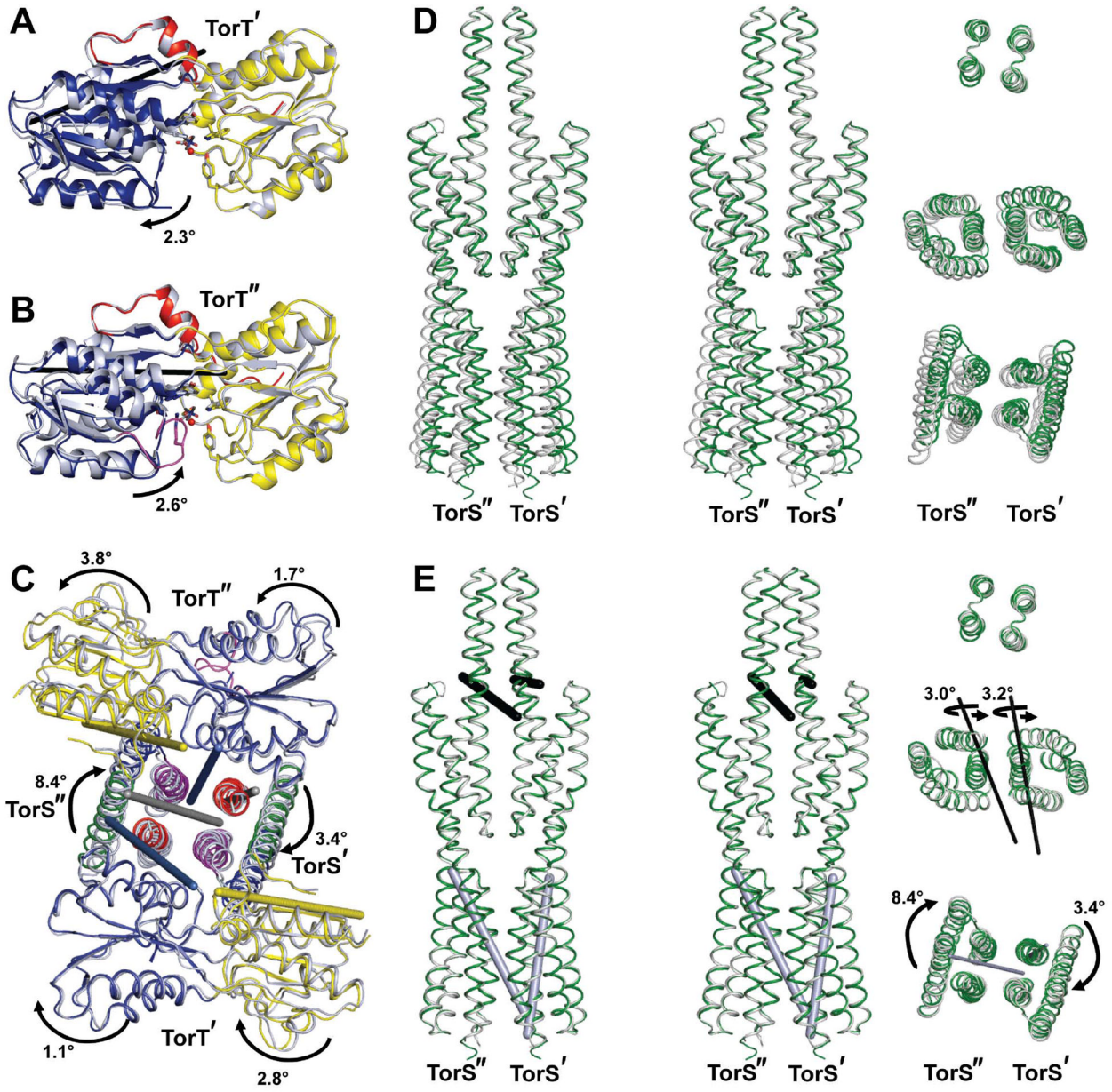

Figure 4. Rigid body motions in vpTorS$_S$-vpTorT complexes

(A) Ribbon diagrams of TorT' (gray) and TorT^T (colored) after superposition of their NTDs. The rotation needed to take the CTD of TorT' into that of TorT^T relative to is indicated as is the axis of that rotation (black rod). The NTD, CTD, and CTE portions of TorT^T are colored yellow, blue, and red respectively.

(B) Ribbon diagrams of TorT" (gray) and TorT^T (colored) after superposition of their NTDs. The rotation needed to take the CTD of TorT" into that of TorT^T is indicated as is the axis of that rotation (black rod). The domains are colored as in 4A except that the ordered TorT" βF-α5 gating loop is in magenta.

(C) Backbone traces of TorT and the proximal bundles of TorS$_S$ from the apo (gray) and TMAO-bound structures (colored) after superposition of the tower bundles. TorT' is on top, TorT" is at the bottom, TorS" is at left, and TorS' is at right. The rotations needed to superimpose the NTDs, CTDs, and the individual proximal bundles from the apo structure

onto the TMAO-bound structure are indicated, as are the axes of the rotations [rods: NTDs (yellow), CTDs (blue), proximal bundles (gray)]. Arrows are directed from apo to ligated states. Coloring is as in 4A and 4B. The view is as in Figure 1B.

(D) Backbone traces of superimposed $TorS_S$-$TorS_S$ dimers. (Left) Stereodiagram of the apo (gray) and TMAO-bound (green) structures after superposition of the tower bundles. The view is as in Figure 1A with TorS" is at left and TorS' is at right. (Right) Cross-sections viewed down the diad-axis of the TMAO-bound structure after 90° rotation as in Figure 1. Segments comprising the tower bundle, the distal bundles, and the proximal bundles (top to bottom, respectively) are positioned at the levels of corresponding segments in the stereodiagram at left.

(E) Backbone traces of $TorS_S$-$TorS_S$ dimers after successive bundle superpositions. (Left) Stereodiagram of the apo (gray) and TMAO-bound (green) structures after successively superimposing the tower bundles, distal bundles, and proximal bundles. The orientation is as in D. (Right) Bundle segments as in D. Rotations needed for the successive superpositions are indicated with arrows directed from apo to TMAO-bound states. The axes of rotation are shown as rods in both left-and right-side diagrams.

See also Table S3 and Figure S4.

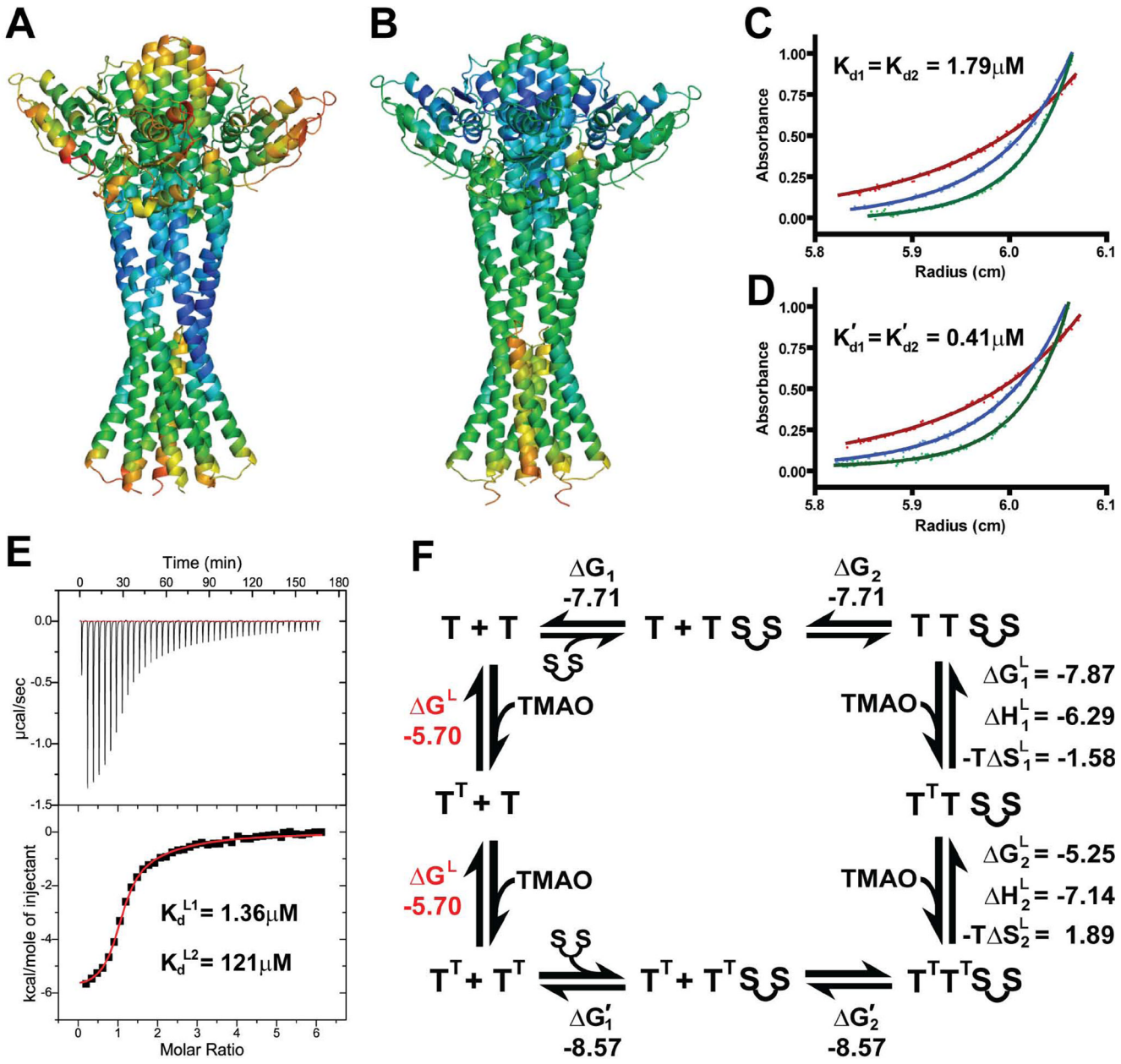

Figure 5. Structural dynamics and thermodynamics formation of TMAO-TorT-TorS$_S$ complexes

(A) Atomic mobilities in the apo TorT-TorS$_S$ complex. Ribbon diagram colored spectrally from blue for the lowest to red for the highest average main chain B-factor. The orientation has the quasi-diad axis vertical as in 1A, but the molecule is rotated by ~50° about that axis whereby TorT' is on the right side and TorT" is on the left.

(B) Atomic mobilities in the TMAO-bound TorT-TorS$_S$ complex. Coloring and orientation are as in A.

(C) AUC data for apo TorT mixed with linked TorS$_S$ dimers. The dots represent measured absorbances (280 nm) for the mixture, starting from the pre-formed 2:1 TorT:TorS$_S$-TorS$_S$ fusion protein complex at ~1.5mg/mL, after sedimentation at 20°C to equilibrium at 10,000 (red), 13,000 (blue), and 16,000 (green) rpm. Superimposed continuous curves are from

fitting by the reversible equilibrium model of T_2:S-S ↔ T + T:S-S ↔ 2T + S-S constrained to identical dissociations, $K_d1 = K_d2 = 1.79$ μM.

(D) AUC data for TMAO-bound TorT mixed with linked $TorS_S$ dimers. Experiments were conducted in the same way with the same proteins as for C, but in 10mM TMAO. Data were analyzed and are displayed as for C, but the fitted dissociation constants here are $K'_{d1} = K'_{d2} = 0.41$ μM.

(E) ITC data for titration of TMAO onto the TorT:$TorS_S$-$TorS_S$ complex. The concentration of the complex was 30 μM and each injection was 5 nl of 1.2mM TMAO (6 nmol). Measurements were made at 20°C. The upper and lower graphs show the raw and integrated data respectively. The red line shows least-squares fit to the integrated data by a two-site sequential binding model. The parameters for binding by the high-affinity site are ΔH= -6.29 kcal/mol, -TΔS= -1.58 kcal/mol, and K_d= 1.36 μM. The parameters for binding by the low-affinity site are ΔH= -7.14 kcal/mol, -TΔS= 1.89 kcal/mol, and K_d= 121 μM.

(F) The thermodynamic cycle for formation of the TorT:$TorS_S$-$TorS_S$ complex and the binding of TMAO. The Gibbs free energy of binding is shown for each step in units of kcal/mol. The value for TMAO binding by uncomplexed TorT (red) was calculated using the law of energy conservation.

See also Figure S5.

Table 1

TorT-TorS$_S$ Refinement Statistics

Parameter	Iso TorT-TorS$_S$	TMAO TorT-TorS$_S$	apo TorT-TorS$_S$
Bragg spacings (Å)	20-2.95	20-3.1	50-2.8
Space Group	$P2_12_12_1$	$C222_1$	$C222_1$
Cell parameters a, b, c (Å)	78.44, 126.67, 306.53	128.06, 306.98, 78.70	115.71, 364.52, 80.81
Z_a	2 TorT; 2 TorS	1 TorT; 1 TorS	2TorT; 2TorS
Solvent content (%)	79.0	79.2	62.2
R_{work} [a] (%)	22.6	21.8	24.8
R_{free} [b] (%)	24.9	25.2	29.1
Number of Reflections	64373	27210	42611
Number of total atoms (nonhydrogen)	9121	4594	9139
Number of protein atoms	9072	4518	9020
Ordered residues	T: 30-171; 176-329 S: 50-319	T: 30-171; 176-329 S: 50-319	T': 30-171; 176-329 T": 30-329 S': 49-318 S": 49-317
Number of water atoms	41	71	98
Number of ligand atoms	8 (2-propanol)	5 (TMAO)	21 (polyethylene glycol)
Average B factor (Å^2)	56.0	49.3	65.8
Rms bond ideality (Å)	0.008	0.009	0.008
Rms angle ideality (°)	1.4	1.4	1.2
Rotamer outlier (%) [c]	9.33	8.76	4.20
Ramachandran (favored/outlier) (%) [c]	87.74/2.04	90.89/0.89	89.92/1.65
PDB code	3O1J	3O1H	3O1I

[a] $R = (\Sigma \mid\mid F_O \mid - \mid F_C \mid\mid) / \Sigma \mid F_O \mid$, where F_O and F_C denote observed and calculated structure factors respectively

[b] R_{free} was calculated using 5% of data excluded from refinement

[c] Molprobity analysis (http://molprobity.biochem.duke.edu/)

See also Table S1 and Figure S1.

Table 2

Dimeric Diad Complexes of Histidine Kinase Receptors

Sensor	Ligand	Symmetry	Equivalent Activity
TorS-TorT	Apo	Asymmetric	Phosphatase (Ansaldi et al., 2001)
	TMAO	Symmetric	Kinase (Jourlin et al., 1997)
Tar	Apo	Symmetric	CheA Kinase (Ninfa et al., 1991)
	Aspartate	Asymmetric (Milburn et al., 1991; Yeh et al., 1993; Yeh et al., 1996)	CheZ Phosphatase (Kim et al., 2001)
NarX	Nitrate	Symmetric (Cheung and Hendrickson, 2009)	Kinase (Williams and Stewart, 1997)
CitA	Citrate	Symmetric (Sevvana et al., 2008)	Kinase (Bott et al., 1995)
DcuS	Malate	Symmetric (Cheung and Hendrickson, 2008)	Kinase (Janausch et al., 2002)
BphP	Pfr State	Asymmetric (Yang et al., 2008)	Phosphatase (Bhoo et al., 2001)
	Q188L mutant	Symmetric (Yang et al., 2009)	Mixed States
PhoQ	Undefined	Quasi Symmetric (Cheung et al., 2008)	Undefined
LuxP-LuxQ	AI-2	Asymmetric (Neiditch et al., 2006)	Phosphatase (Freeman and Bassler, 1999)